

RESEARCH ARTICLE

Vimar Is a Novel Regulator of Mitochondrial Fission through Miro

Lianggong Ding^{1,2}, Ye Lei^{1,2}, Yanping Han², Yuhong Li², Xunming Ji^{2*}, Lei Liu^{2*}

1 State Key Laboratory of Membrane Biology, School of Life Sciences, Peking University, Beijing, China, **2** Aging and Disease lab of Xuanwu Hospital and Beijing Institute for Brain Disorders, Capital Medical University, Youanmen, Beijing, China

* jixunming@vip.163.com (XJ); leiliu@ccmu.edu.cn (LL)



CrossMark
click for updates

 OPEN ACCESS

Citation: Ding L, Lei Y, Han Y, Li Y, Ji X, Liu L (2016) Vimar Is a Novel Regulator of Mitochondrial Fission through Miro. *PLoS Genet* 12(10): e1006359. doi:10.1371/journal.pgen.1006359

Editor: Nils-Göran Larsson, Max Planck Institute for Biology of Ageing, GERMANY

Received: April 1, 2016

Accepted: September 12, 2016

Published: October 7, 2016

Copyright: © 2016 Ding et al. This is an open access article distributed under the terms of the [Creative Commons Attribution License](https://creativecommons.org/licenses/by/4.0/), which permits unrestricted use, distribution, and reproduction in any medium, provided the original author and source are credited.

Data Availability Statement: All relevant data are within the paper and its Supporting Information files.

Funding: This work is supported by the Chinese Ministry of Science and Technology (Grant No. 2013CB530700; <http://www.most.gov.cn/>) to LL and the National Science Foundation (Grant No. 81325007; <http://www.nsf.gov.cn/>) for Distinguished Young Scholars to XJ. The funders had no role in study design, data collection and analysis, decision to publish, or preparation of the manuscript.

Abstract

As fundamental processes in mitochondrial dynamics, mitochondrial fusion, fission and transport are regulated by several core components, including Miro. As an atypical Rho-like small GTPase with high molecular mass, the exchange of GDP/GTP in Miro may require assistance from a guanine nucleotide exchange factor (GEF). However, the GEF for Miro has not been identified. While studying mitochondrial morphology in *Drosophila*, we incidentally observed that the loss of *vimar*, a gene encoding an atypical GEF, enhanced mitochondrial fission under normal physiological conditions. Because Vimar could co-immunoprecipitate with Miro *in vitro*, we speculated that Vimar might be the GEF of Miro. In support of this hypothesis, a loss-of-function (LOF) *vimar* mutant rescued mitochondrial enlargement induced by a gain-of-function (GOF) *Miro* transgene; whereas a GOF *vimar* transgene enhanced *Miro* function. In addition, *vimar* lost its effect under the expression of a constitutively GTP-bound or GDP-bound Miro mutant background. These results indicate a genetic dependence of *vimar* on Miro. Moreover, we found that mitochondrial fission played a functional role in high-calcium induced necrosis, and a LOF *vimar* mutant rescued the mitochondrial fission defect and cell death. This result can also be explained by *vimar*'s function through Miro, because Miro's effect on mitochondrial morphology is altered upon binding with calcium. In addition, a *PINK1* mutant, which induced mitochondrial enlargement and had been considered as a *Drosophila* model of Parkinson's disease (PD), caused fly muscle defects, and the loss of *vimar* could rescue these defects. Furthermore, we found that the mammalian homolog of Vimar, RAP1GDS1, played a similar role in regulating mitochondrial morphology, suggesting a functional conservation of this GEF member. The Miro/Vimar complex may be a promising drug target for diseases in which mitochondrial fission and fusion are dysfunctional.

Author Summary

Mitochondrial dynamics including fusion, fission and transport are essential for energy supply in eukaryotic cells; and defects in mitochondrial dynamics often result in premature aging and diseases such as Parkinson's disease (PD). In mitochondrial transport

Competing Interests: The authors have declared that no competing interests exist.

machinery, the Miro/Milton complex loads mitochondria onto microtubule through kinesin motor proteins; and regulates mitochondrial fusion and fission through unknown mechanisms. As a small GTPase, the exchange of GTP/GDP in Miro requires a specific guanine nucleotide exchange factor (GEF). However, the GEF for Miro has not been identified. In this study, we identified Vimar as a new regulator of mitochondrial dynamics in *Drosophila*. We found that loss of *vimar* promoted mitochondrial shortening; and this function was mediated through Miro. As a GEF, Vimar partially localized on mitochondria and could physically interact with Miro. In the pathophysiological conditions, including a *Pink1* mutant to model PD and a calcium-overload induced stress to model neuronal necrosis in *Drosophila*, loss of *vimar* suppressed both aberrant mitochondrial fusion and fragmentation in PD and necrosis, respectively. As the mammalian homolog of Vimar, RAP1GDS1 function was similar to Vimar. Therefore, Vimar/ RAP1GDS1 may be a great drug target to deal with diseases caused by defective mitochondrial dynamics.

Introduction

Mitochondrial fission, fusion and transport play important roles for the function of this organelle [1, 2]. The balance between fusion and fission controls mitochondrial morphology, which is mediated by series of large dynamin-related GTPases [3]. Among these GTPases, mitofusin1/mitofusin2 (MFN1/MFN2) and optic atrophy protein1 (OPA1) are the core components that are responsible for mitochondrial fusion [4–7], whereas dynamin-related protein 1 (Drp1) is the core component that is responsible for mitochondrial fission [8, 9]. In addition to these GTPases in dynamin-related family, mitochondrial Rho (Miro), an atypical member of the Rho small GTPase family, has a well-known function of transporting the mitochondria along microtubules [10, 11]. Miro also regulates mitochondrial morphology via inhibition of fission under physiological Ca^{2+} conditions, although the mechanism is not that clear [12–16]. Large GTPases such as dynamin-like GTPase family members hydrolyze GTP and exchange GTP and GDP without the assistance from other regulators [17, 18]. However, members of the small GTPase family often require other proteins to help release their tightly bound GDP or enhance their low GTPase activities. These proteins are referred to as guanine nucleotide exchange factors (GEFs) and GTPase activating proteins (GAPs), respectively [19]. To date, most small GTPases require unique GEFs or GAPs [19].

An understanding of the regulation of mitochondrial dynamics may help us to address many human diseases. For instance, mutations in OPA1 or MFN2 result in dominant optic atrophy or Charcot-Marie-Tooth neuropathy type 2A [20, 21]. Abnormal mitochondrial fission also promotes aging and cell death [22, 23]. In necroptosis, the formation of the necrosome promotes mitochondrial fission through dephosphorylation of Drp1 [24]. In neuronal excitotoxicity, calcium ions are overloaded, resulting in reduced levels of the MFN2 protein, which enhances mitochondrial fission and leads to neuronal necrosis [25, 26]. In addition, other components such as Miro may participate in this process [26]. Miro has two EF hand motifs that bind calcium; thus, Miro can couple calcium increase with reduced mitochondrial motility to meet the locally increased energy demands [16, 27]. Interestingly, Miro also promotes fission in the presence of excess calcium, which is distinct from its inhibitory role in fission under normal calcium concentrations [16]. It is unclear whether Miro plays a functional role in neuronal necrosis [26].

The mitochondrial morphology represents a transient balance between mitochondrial fusion and fission [28]. Using a systematic genetic screen in yeast covering approximately 88%

of genes, 117 genes that regulate mitochondrial morphology were identified [29]. Similarly, a screen of 719 genes that are predicted to encode mitochondrial proteins in worms demonstrated that more than 80% of these genes regulate mitochondrial morphology [30]. Although many genes may regulate mitochondrial morphology, their relationships to the core mitochondrial fusion and fission components are unclear.

In studying mitochondrial morphology, we accidentally discovered that the loss of *vimar* (visceral mesodermal armadillo-repeats), which encodes an atypical GEF [31–33], promoted mitochondrial fission in *Drosophila* flight muscle cells. Furthermore, we found that *vimar* was capable of interacting with Miro *in vitro*. Genetically, *vimar* required normal GDP- or GTP-bound activity of Miro to affect mitochondrial morphology, suggesting *vimar* is likely the Miro GEF. In addition, we found that the Miro/*vimar* complex suppressed mitochondrial fission during necrosis and mitochondrial fusion in *PINK1* mutant model of Parkinson's disease (PD), making *vimar* a potential drug target.

Results

Vimar is a novel regulator of mitochondrial morphology in *Drosophila* under normal conditions

To identify novel regulators of mitochondrial morphology, we studied the flight muscle in *Drosophila* adults, because they have a stereotypic distribution of mitochondria in the longitudinal myofibers [34]. To visualize the mitochondria in the muscle cells, a muscle-specific promoter, *Mhc-Gal4*, was used to drive a mitochondria-targeted GFP (*UAS-mitoGFP*); the progenies were referred to as *Mhc>mitoGFP*. The mitochondrial morphology was clearly observed (Fig 1Aa and 1Af). Using these flies, we accidentally observed that mitochondrial fission was enhanced when a *vimar* (*visceral mesodermal armadillo-repeats*) RNAi was expressed (Fig 1Ab and 1Af). To further confirm the loss-of-function (LOF) effect of *vimar*, we tested *vimar*^{k16722}, a P-element mutant with the mobile element inserted into the 5'-UTR region of the *vimar* gene. Again, we observed the trend of enhanced mitochondrial fission in the heterozygous *vimar*^{k16722} mutant (Fig 1Ac and 1Af). Because the homozygous *vimar*^{k16722} mutant was embryonic lethal, we selected a deficient mutant (*Df(2R)ED1612*) covering the *vimar* locus and generated a trans-heterozygous *vimar* (*vimar*^{k16722}/*Df*) mutant to further test the effect of *vimar*. In these flies, the mitochondria exhibited a stronger fission morphology compared to the heterozygous mutant (Fig 1Ad and 1Af). These results indicate that *vimar* plays a dominant role in regulating mitochondrial morphology in a dosage-dependent manner. To confirm the mitochondrial defect was generated from loss of *vimar*, we tried to rescue *vimar*^{k16722}/*Df* by *tubulin-Gal4/UAS-vimar* (*tubulin-Gal4* is a ubiquitously expressed promoter). The result showed that the shortened mitochondria in the *vimar*^{k16722}/*Df* mutant were rescued by *vimar* overexpression (S1A Fig); while overexpression of *vimar* alone did not affect the mitochondrial morphology (Fig 1Ae and 1Af), suggesting that the levels of the *vimar* protein may be saturated under normal physiological condition. Using a polyclonal antibody of *vimar*, we confirmed that the protein levels of *vimar* were reduced in *vimar*^{k16722} and *vimar* RNAi, and increased in the *vimar* overexpression line (S1B and S1C Fig).

To examine mitochondrial distribution, we studied *Drosophila* larval oenocytes because of their stereotypical location and morphology. The wild type mitochondria, labeled with *UAS-mitoGFP* driven by an oenocytes-specific promoter, *PromE(800)-Gal4*, were evenly distributed in the cytosol (Fig 1Ba). As positive controls, we knocked down *Khc* (kinesin heavy chain), *Milton* (an adaptor protein to link *Khc* to mitochondria) and *Miro*, which are the core components of mitochondrial transport machinery [35]. The results showed that mitochondrial spreading was greatly reduced in the cytosol, and resulted in accumulation in the perinuclear region

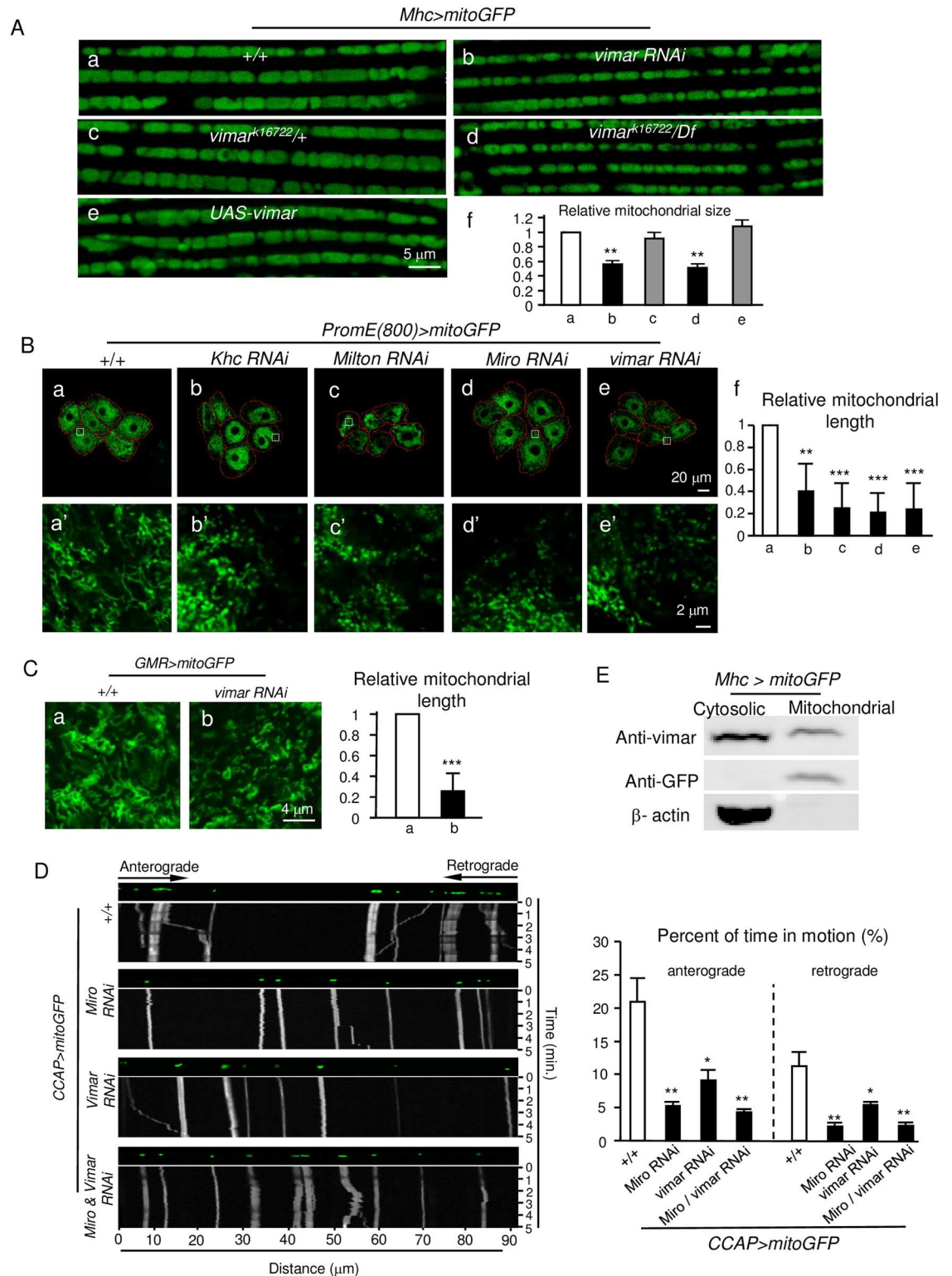


Fig 1. *Drosophila vimar* affects mitochondrial morphology under normal conditions. (A) a-e, Live imaging of the mitochondrial morphology in the flight muscle of adult flies. The mitochondria are labeled with *UAS-mitoGFP* driven by *Mhc-Gal4* (*Mhc>mitoGFP*). The genotype is indicated on each micrograph. f, To quantify the mitochondrial size, the averaged mitochondrial size of the control (*+/+*) is set as 1, and the relative ratios of the other genotypes to the control are shown. Five thoraces from each genotype were quantified. Bar graphs throughout all figures are means \pm SD. The white

bar represents the control, the gray bar represents no statistical different from the control, and the black bar represents significantly different from the control. * for $p < 0.05$; ** for $p < 0.01$; *** for $p < 0.001$. (B) Mitochondrial distribution and morphology in larval oenocytes. a, The mitochondria are labeled with *PromE(800) > mitoGFP*. b-e, The effects of *Khc*, *Milton*, *Miro* and *vimar RNAi* are shown. The dotted red lines denote the cell boundaries, which were determined by the mitoGFP background. a'-e', Enlarged view of the white box labeled area in the upper panel. f, To quantify the mitochondrial length, the averaged mitochondrial length of the control (+/+) is set as 1, and the relative ratios of the other genotypes to the control are shown. Mitochondrial length of five oenocytes was quantified per genotype and shown as means \pm SD. (C) Live imaging of mitochondria in eye disc after knocking down *vimar* by *GMR > mitoGFP*. Three eye discs were analyzed for each genotype. (D) Effect of *vimar* on mitochondrial transport. The mitochondria are labeled with mitoGFP (*CCAP > mitoGFP*), and their movements in the axons were recorded and transformed into kymographs. Mitochondria motion in ten axons from five larvae was analyzed for each genotype. The quantification is shown on the bar graph. (E) Subcellular vimar protein distribution by protein fractionation. The proteins from adult thoraces (*Mhc > MitoGFP*) were separated into cytosolic and crude mitochondrial fractions. The vimar protein enrichment was analyzed by immunoblotting with the anti-vimar antibody. The mitoGFP protein was detected by the anti-GFP antibody; and β -actin is a cytosolic protein.

doi:10.1371/journal.pgen.1006359.g001

(Fig 1Bb–1Bd). Interestingly, knocking down *vimar* by RNAi showed a similar distribution pattern (Fig 1Be). For mitochondrial morphology, loss of *Khc*, *Milton*, *Miro* and *vimar* resulted in mitochondrial shortening (Fig 1Ba'–1Be' and 1Bf). Similarly, mitochondria in the eye disc of *GMR > mitoGFP/vimar RNAi* was also shortened (Fig 1C). These results suggest that vimar regulates mitochondrial morphology in different cell types, such as muscle, oenocyte and eye disc.

Transport of mitochondria along the axon can be quantified in *Drosophila* neurons *in vivo* [36]. As a positive control, the *CCAP-Gal4 > Miro RNAi* line (*CCAP-Gal4* is a promoter labeling a single axon within a neuron bundle) displayed reduced flux of mobile mitochondria in both anterograde (soma to synapse) and retrograde (synapse to soma) transport (Fig 1D). The *CCAP-Gal4 > vimar RNAi* line showed a similar result (Fig 1D). RNAi of both *vimar* and *Miro* resulted in a similar reduction of mitochondrial transport as *Miro* RNAi alone (Fig 1D), suggesting vimar and Miro may function in the same pathway.

To test vimar subcellular localization, proteins from the thoraces of adult flies (*Mhc > MitoGFP*) were extracted and separated into cytosolic and mitochondrial fractions. The Western blot data showed that endogenous vimar was present in both cytosol and mitochondria (Fig 1E). Apart from mitochondria, to test whether Vimar can distribute in other subcellular compartments, we fractionized organelles of ER, lysosome and Golgi apparatus, and found that Vimar was also enriched in the ER fraction, as well as in the cytosol (S2A Fig). This result is consistent with reports suggesting that Miro protein is localized and function in the site of mitochondria-ER junction [37, 38].

Vimar functions through Miro to regulate mitochondrial morphology

We asked whether vimar regulates mitochondrial morphology through controlling the GTP/GDP exchange of Miro, because Miro is a well-known small GTPase that regulates mitochondrial transport and morphology [10, 14].

First, we evaluated their physical interactions. The Flag-tagged Vimar (Vimar-Flag) and HA-tagged Miro (Miro-HA) were ectopically expressed in the HEK293T cells. By co-immunoprecipitation (co-IP) assays with anti-HA and anti-Flag antibodies, Miro and Vimar could pull down with each other (Fig 2A). This result suggests that Miro and Vimar can bind with each other, at least under the overexpression conditions.

Next, we tested their genetic interactions. The wing posture defects underline dysfunctional flight muscles that control wing position and movement [39]. It has been reported that overexpression of Miro induces mitochondrial enlargement [13, 15, 16]. Consistently, we observed this mitochondrial change in the Miro overexpression condition. Meanwhile, the wing posture defects of *Mho > Miro* flies increased progressively after eclosion and reached the maximum to

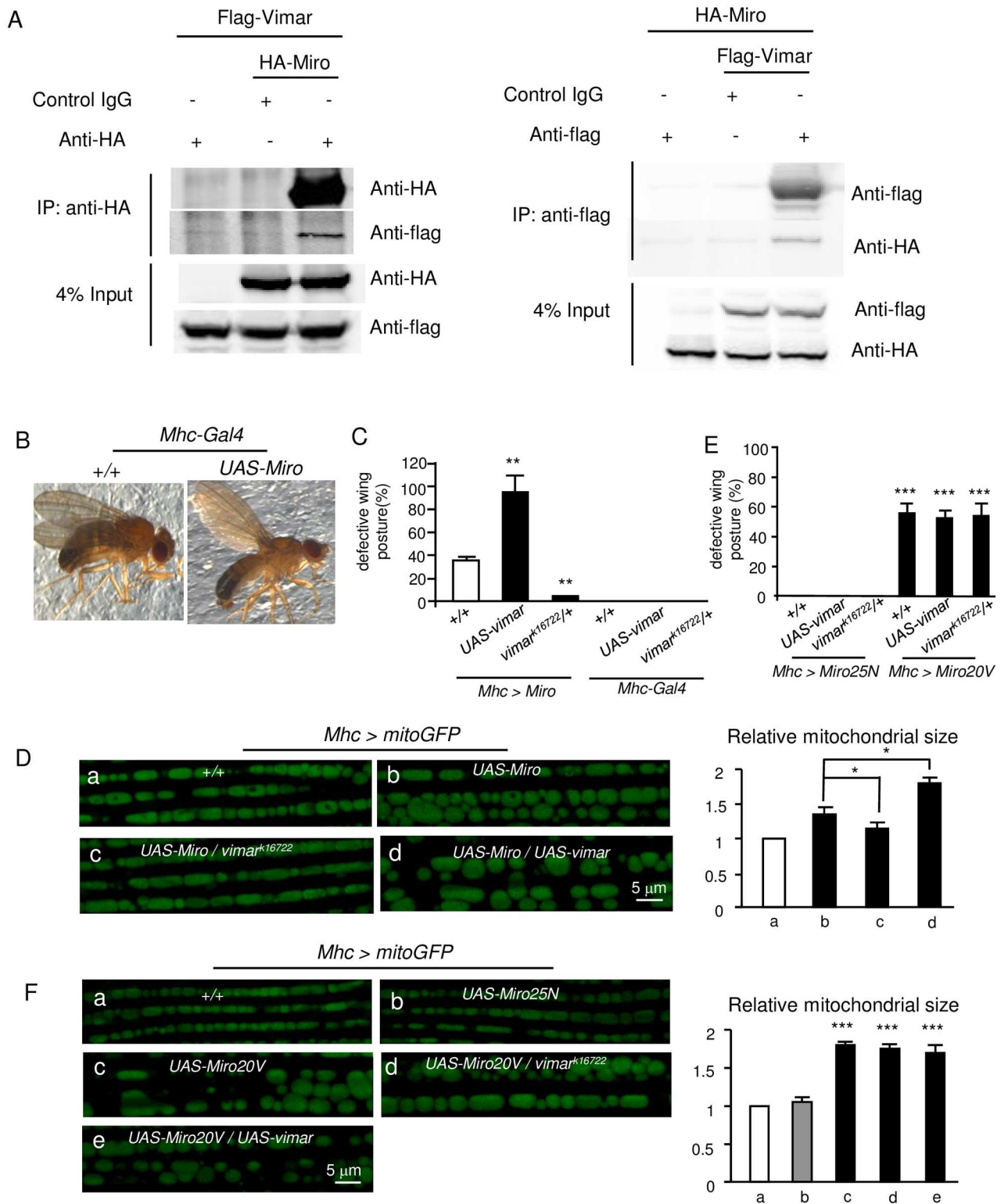


Fig 2. Interaction of vimar and Miro. (A) Co-immunoprecipitation of vimar and Miro. The proteins were collected from the HEK293T cells that expressed both Flag-tagged Vimar (Flag-Vimar) and HA-tagged Miro (HA-Miro). Then, the proteins were precipitated with a HA (left panel) or Flag antibody (right panel). The control IgG is shown as a negative control. The total protein input is shown as the protein loading control. (B) An example of the defective wing posture. Compared to the control, overexpression of *Miro* in the adult flight muscle (*Mhc*>*Miro*) resulted in an upright fly wing posture. (C) Quantification of defective wing posture in the *Miro* overexpression background or

in the *Mhc-Gal4* background. Trial N = 3, with 100–150 flies examined in each experiment. (D) Live imaging of the mitochondrial morphology in the fly flight muscle. The genotype of each fly muscle is labeled on the micrograph. Five thoraces were quantified for each genotype. (E) Quantification of defective wing posture in the Miro20V and Miro25N overexpression background. Trial N = 3, with 100–150 flies examined in each experiment. (F) Live imaging of the mitochondrial morphology in the fly flight muscle in the indicated genotypes. Five thoraces were quantified for each genotype.

doi:10.1371/journal.pgen.1006359.g002

approximately 30% at the seventh day after eclosion (Fig 2B and 2C). Interestingly, *vimar*^{k16722} almost completely abolished the wing defect induced by the *Miro* overexpression; while *vimar* overexpression greatly enhanced the wing posture defect. As controls, *vimar* overexpression alone or *vimar* mutant (*vimar*^{k16722}) had no wing posture defect (Fig 2C). For the mitochondrial morphology in the *Mhc>mitoGFP* flies, *Miro* overexpression resulted in aberrant mitochondrial size enlargements (Fig 2Da and 2Db), and these defects could be rescued by the heterozygous *vimar*^{k16722} mutant (Fig 2Dc). Moreover, *vimar* overexpression further enhanced mitochondrial size increase under the *Miro* overexpression background (Fig 2Dd). These results suggest that *vimar* may genetically interact with *Miro*.

We cannot test effect of GOF *vimar* under the *Miro RNAi* background, because *Miro RNAi* did not induce the wing posture defects in the flight muscles. To further test *Miro/vimar* interaction, we generated transgenes of constitutively GDP-bound or GTP-bound mutant of *Miro*. The rationale is that GOF or LOF *vimar* should not affect these mutant phenotypes if *vimar* functions as a *Miro* GEF. Based on a previous report [40], the amino acid substitutions of A20V (*Miro20V*) and T25N (*Miro25N*) should render *Miro* constitutively GTP-bound and GDP-bound, respectively. As expected, a *Miro25N* overexpression in the flight muscle (*Mhc>Miro25N*) did not affect the wing posture (Fig 2E) or mitochondria morphology (Fig 2Fa and 2Fb). In contrast, a strong wing posture defect (Fig 2E) and enlarged mitochondria size (Fig 2Fc) were observed in the *Miro20V* overexpression line (*Mhc>Miro20V*). Importantly, GOF or LOF *vimar* failed to affect the defects in the *Miro20V* overexpression line (Fig 2E, 2Fd and 2Fe). We also examined *vimar* effect on mitochondrial transport in the GOF *Miro*WT, *Miro20V* and *Miro25N* background. However, we found that almost no mitochondria were distributed in the axons in the GOF *Miro*WT or *Miro20V* background. This data is consistent with previous reports indicating GOF *Miro* strongly increased mitochondrial length and reduced transportation [41, 42]. We could not examine their mitochondrial transports. In contrast, mitochondrial transport was unaltered under GOF *vimar* background or combined with *Miro25N* expression (S2B Fig). Together, these results suggest that *vimar* requires the normal GTP/GDP binding activity of *Miro* for its function.

To test whether the *vimar/Miro* interaction depends on the GTPase activity of *Miro*, we co-transfected *vimar*-Flag with inactive (*Miro25N*) and active (*Miro20V*) form of *Drosophila* HA-*Miro* in the HEK293T cells. The co-IP results showed that the *vimar/Miro* interaction was unaffected by these *Miro* mutants (S2C Fig). This result suggests that *Miro/vimar* interaction is not regulated by the GTPase activity of *Miro*. For mitochondrial distribution of *vimar* under the LOF *Miro* background (*Mhc>mitoGFP/Miro RNAi*), we observed that the mitochondrial fraction of *vimar* was unaltered (S3A Fig). This result indicates that *vimar* may attach with mitochondria by itself or with other partners.

It has been reported that mitochondrial shortening caused by *Miro* loss required the function of Drp1 [16]. Therefore, we could expect that loss of Drp1 might rescue the mitochondrial shortening in the muscle of *Miro RNAi* background. Indeed, it is the case (S3B Fig). Regarding the interaction between Drp1 and *Vimar*, our data showed that loss of Drp1 also rescued the mitochondrial shortening of the *Vimar* mutant (S3B Fig). This result indicates that *Miro/Vimar* complex is likely to regulate mitochondrial fission through Drp1.

To study whether Miro/vimar affected the Drp1 recruitment to mitochondria under *Miro RNAi* or *vimar RNAi* backgrounds, we used a transgene with a 9.35 kb genomic DNA insertion, which contains an endogenous Drp1 gene labeled by a HA tag (Flag-FLAsH-HA-Drp1) [43, 44]. The result showed that the mitochondria fraction of Drp1 monomer was unaltered in these RNAi conditions (S3C and S3D Fig). This result indicates that loss of Miro/vimar may not affect the recruitment of Drp1 to mitochondria, and how Miro/vimar affects Drp1 function is unclear.

Vimar promotes mitochondrial fission in response to high calcium concentrations

Miro plays distinct roles in regulating mitochondrial morphology under normal and high calcium conditions [16]. In normal conditions, Miro increases mitochondrial size through inhibition of Drp1 function [13, 15, 16]; however, it promotes mitochondrial fission in high calcium conditions by increasing Drp1 activity, such as in depolarized neurons [16, 35]. If vimar functions through Miro, we expect that vimar may promote mitochondrial fission in high calcium conditions.

To test Miro/vimar response at high calcium state, we had previously established a fly model to study the high calcium-induced cellular response, and accomplished calcium overload by expressing a leaky cation channel, the glutamate receptor 1 Lurcher mutant (GluR1^{Lc}) [45, 46]. This fly model (simplified as the AG model) contained *Appl-Gal4* (a neuron-specific promoter), *UAS-GluR1^{Lc}* and *tub-Gal80^{ts}* (an inhibitor of Gal4 at 18°C, which lost its function at 30°C). Thus, the AG flies were normal at 18°C, and calcium overload was induced upon a shift to 30°C [45]. Following the time progression after the GluR1^{Lc} induction, calcium accumulates and neuronal necrosis increases gradually in the AG flies [45].

It is well known that mitochondrial fragmentation occurs upon calcium overloaded [47]. To recapitulate this phenomenon and observe mitochondrial morphology by live cell imaging, we added *UAS-mitoGFP* to the AG flies (simplified as the AGM model). After the AGM larval flies were raised at 30°C to induce calcium influx for 20 hours, mitochondrial fragmentation in the chordotonal neurons showed subtle fission compared to control; while at the 26 hour, the mitochondria in the AGM dendrites underwent dramatic fragmentation (Fig 3A–3D). For the rescue effect of a given genetic manipulation, we showed the 26 hour time point (to rescue the more severe defects); and for the enhancer effect of a given genetic manipulation, we showed the 20 hour time point (to enhance a less defective phenotype). As a positive control, a LOF mutant of Drp1, *drp1¹*, which possessed an A186V amino acid substitution at the Dynamin-GTPase domain [44], strongly suppressed the mitochondrial fission defect (Fig 3Ac and 3Ad). These results suggest that the AGM model can be adopted to study the mitochondrial morphology in high calcium conditions.

Because Miro promotes mitochondrial fission in the high calcium conditions [16], we expected that vimar might enhance Miro function under high calcium concentrations; and the LOF *vimar* might rescue the mitochondrial fission defect in the AGM flies. Indeed, GOF *vimar* enhanced mitochondrial fission (Fig 3Bb and 3Bc); and *vimar^{k16722}* rescued mitochondrial fission in the AGM flies (Fig 3Cb and 3Cc). In the high calcium state, the mitochondrial localization of vimar was unaltered (S4 Fig), indicating recruitment of vimar on mitochondria is likely independent on calcium level. To further test the role of Miro/vimar complex, we examined effect of the GOF *Miro* transgene in the *vimar^{k16722}* background. The result demonstrated that the GOF *Miro* enhanced mitochondrial fission (Fig 3Db and 3Dc), whereas *vimar^{k16722}* could not rescue the defect (Fig 3Dd), indicating that basal function of Miro may be partially independent from vimar. Together, these results suggest that vimar functions through Miro to regulate mitochondrial morphology in high calcium conditions.

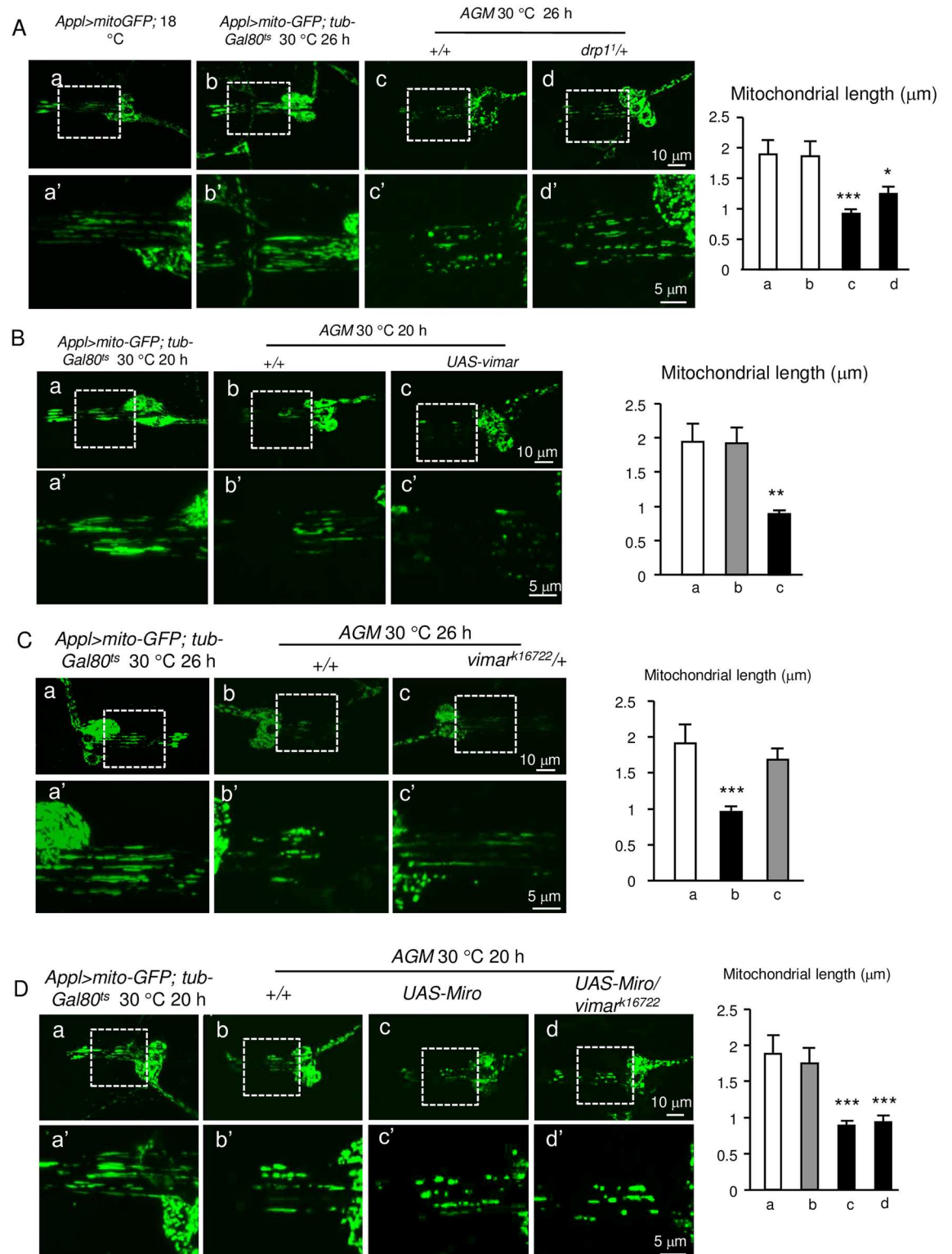


Fig 3. Vimar modulates the mitochondrial length in the high calcium condition. (A) Effect of the Drp1 mutation on mitochondrial fission in high calcium conditions. **a** and **b**, Mitochondrial dendrites in the larval chordotonal neurons in the control flies (*Appl>mitoGFP* at 18 °C and *Appl>mitoGFP, tub-Gal80^{ts}* at 30 °C). **c** and **d**, Mitochondrial morphology in the *AGM* and *AGM/drp1¹* flies. **a'**-**d'** are the enlarged view from the boxed area in **a**-**d**, and the mitochondrial lengths in **a'**-**d'** were quantified. 10 to 16 chordotonal organs from each genotype were examined. **(B)** Effect of the *vimar* overexpression

on the mitochondrial length after induction of *AGM* expression for 26 hours. 10 to 16 chordotonal organs were examined for each genotype. (C) Effect of *vimar* mutant (*vimar*^{k16722}) on the mitochondrial fragmentation of the *AGM* flies. 10 to 16 chordotonal organs were examined for each genotype. (D) Effect of *Miro* overexpression and the *vimar* mutant on the mitochondrial fragmentation of the *AGM* flies. 10 to 16 chordotonal neurons were examined for each genotype.

doi:10.1371/journal.pgen.1006359.g003

The loss of *vimar* suppressed both necrotic cell death and muscle defects in a *Drosophila* PD model

Mitochondrial fission may enhance calcium overload-induced necrotic cell death in neuron cultures [47]. However, there is still insufficient genetic evidence to demonstrate that mitochondrial fission plays a causal role in neuronal necrosis [48]. To study this question, we previously showed that we could quantify necrosis in the *AGG* flies (the *AG* flies containing *UAS-GFP*) at single cell resolution [45]. The result showed that *Drp1*¹ could rescue necrosis in the chordotonal neurons (Fig 4A). In addition, the function of these neurons could be assessed at the behavioral level by quantifying adult fly death [45]; *Drp1*¹ rescued the lethality of the *AG* flies (Fig 4B). Strikingly, *vimar*^{k16722} exhibited a rescue effect in the *AGG* flies at both the cellular and behavioral levels (Fig 4C and 4D). In contrast, the GOF *vimar* transgene had the opposite effect (Fig 4E and 4F). This result is consistent with the suppression of mitochondrial fission in this mutant. Furthermore, the GOF *Miro* transgene enhanced necrosis; however, *vimar*^{k16722} did not rescue the GOF *Miro* phenotype (Fig 4G and 4H), similar to its effect on mitochondria. These results indicate that Miro has the dominant role in the Miro/*vimar* complex and that the Miro/*vimar* complex plays a functional role in neuronal necrosis.

In the *PINK1* mutant of the Parkinson's disease (PD) *Drosophila* model, mitochondrial fusion is enhanced, and the LOF *Miro* mutant could suppress this mitochondrial defect [13]. Therefore, we speculate that the LOF *vimar* mutant might rescue the defective mitochondrial fusion in the *PINK1* mutant. To test this hypothesis, we studied a *PINK1* mutant, *PINK1*⁵ [49]. In the *PINK1*⁵ flies, the mitochondria are abnormally elongated and fused (Fig 4I), and the fly wing posture is defective (Fig 4J). Strikingly, *vimar*^{k16722} could rescue both the mitochondrial morphology and wing posture defects (Fig 4I and 4J). Together, these results indicate that LOF of the Miro/*vimar* complex suppressed both mitochondrial fragmentation during necrosis and *PINK1* mutant of *Drosophila* PD model.

Furthermore, we found that *vimar*^{k16722} and *UAS-vimar* had no effect on classical apoptosis induced by Hid expression [50] (S5 Fig), suggesting that *vimar* may specifically affect PD and necrosis, but does not regulate apoptosis.

The mammalian homolog of *vimar* (RAP1GDS1) plays a similar role in mitochondrial morphology and cell death

A protein sequence comparison showed that *Drosophila* *vimar* shares great similarity with the mammalian protein RAP1GDS1 (S6 Fig); however, it is not clear whether *vimar* is a functional homolog of RAP1GDS1 [51]. Here, we further investigated the role of RAP1GDS1 in mitochondrial morphology. First, we used a lentivirus to transfect a RAP1GDS1 shRNA into HEK293T cells and established a stable cell line. As expected, the protein level of the RAP1GDS1 was significantly reduced in the shRNA line (S7A Fig). Then, this shRNA line was transiently transfected with a mitochondrial reporter, mitoDsRed. We found that the mitochondrial length showed a trend of reduction in the RAP1GDS1 shRNA cells (Fig 5A). Next, we studied the effect of RAP1GDS1 on necrosis. Necrotic cell death was induced by a calcium ionophore (A23187), which causes calcium overloading and necrosis [52]. As expected, the calcium ionophore induced mitochondrial fragmentation, and the RAP1GDS1 shRNA rescued the mitochondrial defect (Fig 5B). To quantify the cell death, we measured cellular ATP level

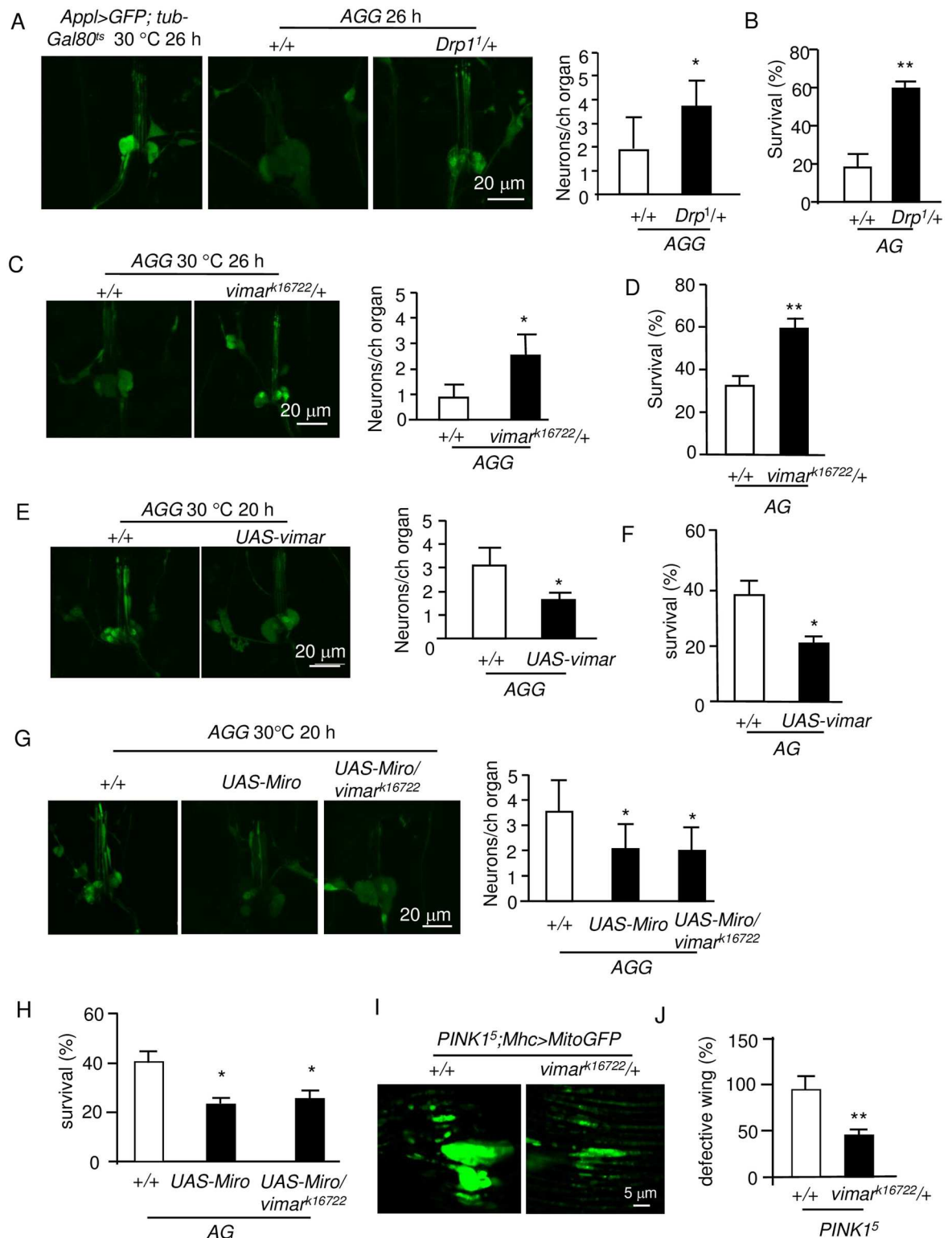


Fig 4. Vimar suppresses neuronal necrosis and muscle degeneration induced by the *Pink1* mutant. (A) Effect of the *Drp1* mutant on neuronal necrosis. The micrographs showed the live images from larval chordotonal neurons. The control (*App1>GFP;tub-Gal80^{ts}*) displays the cell bodies of the wild type chordotonal neurons, which form a cluster containing 6 neurons. In the AGG background, the wild type (*+/+*) flies showed swollen cell bodies, weakened GFP intensity and neuronal cell loss; and these defects were rescued under the *Drp1* mutant (*Drp1¹*) background. The right panel shows the quantification

of the cell loss. For all quantification of neuronal necrosis, trial N = 5, with 10–15 flies were examined in each trial in this figure. (B) Effect of the *Drp1* mutant on the survival of the AG adult flies. For all quantification of AG lethality, trial N = 3, with 100–150 flies were examined for each trial. (C) Effect of *vimar* mutant on neuronal necrosis. (D) Effect of the *vimar* mutant on the survival of the AG flies. (E) Effect of *vimar* overexpression on neuronal necrosis. (F) Effect of *vimar* overexpression on the survival of the AG flies. (G) Effect of *Miro* overexpression on neuronal necrosis. The result showed that *Miro* overexpression enhanced neuronal necrosis; and the *vimar* mutant had no rescue effect on this defect. (H) Effect of *Miro* overexpression on the survival of the AG flies. (I) Effect of the *vimar* mutant (*vimar*^{k16722}) on *PINK1* mutant induced mitochondrial defect. The live image showed the mitochondrial morphology in the *PINK1* mutant (*PINK1*⁵) and under the *vimar* mutant background. Ten thoraces were analyzed for each genotype. (J) Effect of the *vimar* mutant (*vimar*^{k16722}) on the wing posture defect of the *PINK1* mutant (*PINK1*⁵). Trial N = 3, with 100–150 flies were examined in each trial.

doi:10.1371/journal.pgen.1006359.g004

and performed propidium iodide (PI) staining [53]. The result showed that RAP1GDS1 shRNA rescued necrosis in both assays (Fig 5C and 5D). Moreover, we tested the RAP1GDS1 shRNA in another human cell line, the SH-SY5Y neuroblastoma cells. Similar to the HEK293T cells, the RAP1GDS1 shRNA protected the SH-SY5Y cells from calcium overload (S7B and S7C Fig). In addition, we examined the effect of a Miro-1 siRNA on calcium ionophore induced necrosis. The result showed that it also rescued the cell death (Fig 5E and 5F, and the Miro-1 siRNA effect is shown in S7D Fig). Furthermore, the HA-tagged Miro1 and the Flag-tagged RAP1GDS1 could co-immunoprecipitate *in vitro* (Fig 5G). Together, these results indicate that the function of the Miro1/RAP1GDS1 complex in regulating mitochondrial morphology and necrosis is conserved with the *Drosophila* Miro/vimar complex.

Discussion

Vimar is a novel regulator of mitochondrial morphology

Mitochondrial function can be assessed by the enzymatic activity of citrate synthase (CS), the first enzyme in the Krebs cycle that converts acetyl-CoA and oxaloacetate to citrate [54]. In cultured *Drosophila* S2 cells, *vimar* knock down by RNAi resulted in reduced CS activity [54], indicating that *vimar* may positively regulate mitochondrial function. Because mitochondrial fission has generally been associated with reduced mitochondrial respiration [55], the decreased CS activity may be a result of mitochondrial fission. Consistent with this notion, our results demonstrated that the LOF of *vimar* promoted mitochondrial fission. In addition, a GOF *vimar* transgene had a minimal effect on mitochondrial morphology, indicating that *vimar* activity might be saturated under normal physiological conditions.

Vimar functions through Miro to regulate mitochondrial morphology

Because Vimar has been predicted to be a GEF, we hypothesized that *vimar* may regulate mitochondrial morphology by affecting a small GTPase, which requires a GEF to help with the GTP/GDP exchange process [19]. Interestingly, Miro is one such small GTPase that is known to play important roles in mitochondrial fission and transport [10, 14, 16]. We propose that *vimar* and Miro may function as a complex. First, a fraction of the *vimar* protein was localized to the mitochondria, possibly indicating a functional role on mitochondria. Interestingly, the mitochondrial localization of *vimar* seems not dependent on Miro, because LOF Miro did not affect the mitochondrial fraction of *vimar*. This indicates that *vimar* may directly bind with mitochondria or through other scaffolding proteins. Second, *vimar* and Miro could physically interact with each other, at least *in vitro*. Their interaction seems not affected by the GTPase activity of Miro, because the constitutively GDP- or GTP-bound Miro mutants did not affect their interactions. Third, *vimar* genetically interacted with Miro. This included the result demonstrating that the LOF *vimar* mutant reduced the effect of Miro on mitochondrial fission

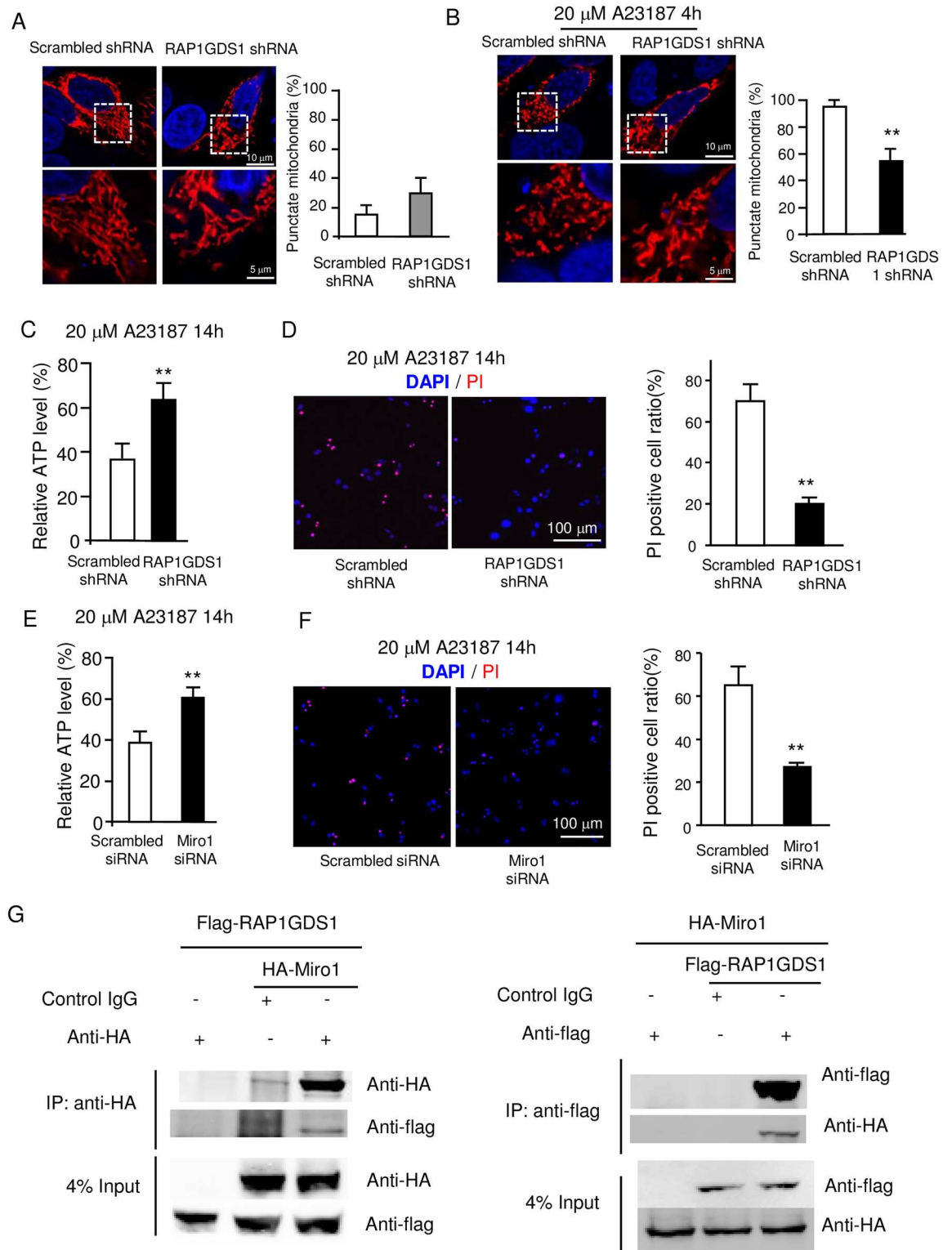


Fig 5. The conserved role of RAP1GDS1 in mammalian cells. (A) Effect of RAP1GDS1 knock down on the mitochondrial morphology in HEK293T cells. The mitochondria in the cells that stably express the RAP1GDS1 shRNA are labeled with a transiently transfected MitoDsred expression vector. The cells were classified as tubular-shape or punctate-shape based on differences in their mitochondrial lengths. The ratio of punctate-shape mitochondria is shown in the right panel. The result showed that RAP1GDS1 shRNA had a trend to increase the punctate-shape mitochondria (not statistically different from the

control shRNA). Trial N = 3, with 100 cells were quantified in each trial. **(B)** Effect of RAP1GDS1 knocking down on the mitochondrial fragmentation under calcium overload stress. The HEK293T cells were treated with 20 μ M calcium ionophore (A23187) for 4 hours. The result showed that RAP1GDS1 shRNA reduced fragmented mitochondria upon calcium ionophore treatment. Trial N = 3, with 100 cells were quantified in each trial. **(C)** Effect of the RAP1GDS1 shRNA on calcium ionophore-induced necrosis. The HEK293T control and RAP1GDS1 shRNA stable cell lines were treated with 20 μ M A23187 for 14 hours. Then, the cell death was quantified by the ATP assay. The result indicated that less cell death occurred in the RAP1GDS1 shRNA expressing cells. Trial N = 3. **(D)** Effect of the RAP1GDS1 shRNA on calcium ionophore-induced necrosis. The PI and DAPI staining patterns are shown. The red signals indicate the PI-positive cells and the blue channel indicates the DAPI staining. Trial N = 3. **(E)** Effect of the *Miro1* siRNA on calcium ionophore induced necrosis determined by the ATP assay. The *Miro1* siRNA was transiently transfected in HEK293T cells for 48 hours. Trial N = 3. **(F)** Effect of the *Miro1* siRNA on calcium ionophore induced necrosis determined by the PI staining assay. The PI and DAPI staining patterns are shown. The same result was observed as in **E**. Trial N = 3. **(G)** Co-Immunoprecipitation of RAP1GDS1 and Miro1. The proteins were collected from the HEK293T cells that expressed Flag-tagged RAP1GDS1 (Flag-RAP1GDS1) and HA-tagged Miro1 (HA-Miro1). The control IgG is shown as a negative control. The total protein input is shown as the protein loading control. Trial N = 3.

doi:10.1371/journal.pgen.1006359.g005

inhibition and the GOF vimar transgene had the opposite effect. Moreover, in the constitutive GFP-bound or GDP-bound Miro mutants, the effect of the GOF or LOF *vimar* was abolished. Therefore, vimar requires the normal GDP/GTP binding activity of Miro to function. It is also known that Miro1 overexpression increase mitochondrial size partially by suppression of the Drp1 function [15, 16]. Consistently, increased mitochondrial fission in the LOF of Miro or vimar was abolished by loss of Drp1, suggesting the Miro/vimar complex depends on Drp1 to regulate mitochondrial morphology.

The Miro/vimar complex may regulate PD and neuronal necrosis through mitochondrial fusion and fission

Familial PD caused by mutations in *PINK1* or *Parkin* results in a series of mitochondrial dysfunctions, particularly the failure to eliminate damaged mitochondria through mitophagy [56, 57]. In these *PINK1* or *Parkin* mutants, the key proteins involved in mitochondrial fusion and fission, such as Marf/Mitofusin and Miro, accumulate [13, 58]. In the *PINK1* mutant flies, the flight muscle is damaged, resulting in wing posture defects [59]. Similarly, we observed that Miro overexpression in the flight muscle resulted in a strong wing posture defect. This result may explain the wing posture defect in the *PINK1* mutant, in which the levels of the Miro protein are increased [13]. Our result demonstrated that the LOF of *vimar* could rescue the wing defect in the *PINK1* mutant, consistent with the hypothesis that vimar functions through Miro.

When the intracellular calcium level is high, Miro switches from promoting mitochondrial fission inhibition to enhancing mitochondrial fission [16]. The mechanism for this switch is unclear, although alterations of Drp1 function could be one possibility [16]. Interestingly, Gem1, the yeast homolog of Miro GTPase, has been reported to function as a negative regulator for ER-mitochondria contacts, where Drp1 aggregates and cleaves mitochondria into smaller units [37]. This may serve as the mechanism for Miro to regulate mitochondrial morphology via Drp1. In addition to affect mitochondrial fission, Miro also regulates mitochondrial transport in a calcium dependent manner. For mitochondrial transport, Miro forms protein complexes with Milton, a kinesin adaptor, and with motor proteins, such as kinesin and dynein [35]. In high calcium conditions, Miro alters its binding patterns and results in reduced transport activity [27, 60, 61]. Based on these reports, we proposed that the Miro/vimar complex acted together to affect mitochondrial morphology: at normal condition, Miro/vimar inhibits fission via Drp1; at high calcium state, Ca²⁺ bound Miro switches its function to promote fission. Indeed, vimar responds to the calcium change in the same way as Miro (Fig 6). In addition, our data demonstrated that knocking down

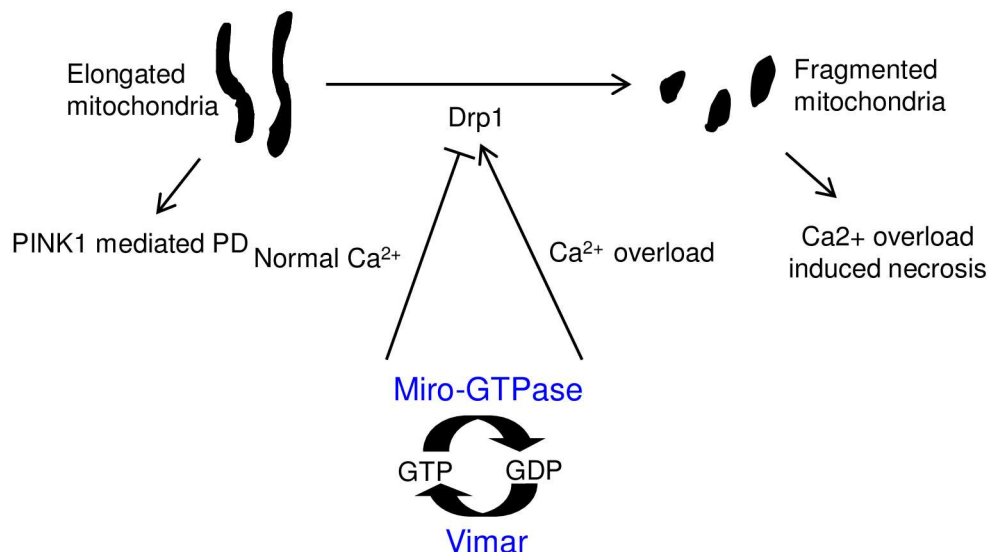


Fig 6. A schematic model of Miro/vimar function on mitochondrial morphology. In normal calcium conditions, the Miro/vimar complex promotes mitochondrial fission inhibition, and their GOF results in elongated mitochondria. Increased mitochondrial fusion is known to occur in the *PINK1* mutant flies, and this defect can be rescued by LOF Miro/vimar. In the high calcium state, the Miro/vimar complex promotes mitochondrial fragmentation, which accelerates neuronal necrosis. Regardless of the intracellular calcium level, vimar enhances the function of Miro, because vimar is likely the GEF to promote Miro's GTP/GDP exchange.

doi:10.1371/journal.pgen.1006359.g006

RAP1GDS1 and Miro1 increased mitochondrial fission and could rescue calcium overload induced necrosis, similar to the loss of vimar or Miro in *Drosophila*. These data support the hypothesis that RAP1GDS1 is the mammalian homolog of vimar, supporting a previous prediction [51].

Mitochondrial fission plays important role in apoptosis by promoting mitochondrial outer-membrane permeabilization (MOMP) to release cytochrome c from the mitochondria [62]. The use of the Drp1 inhibitor mdivi to block fission has been shown to be an effective treatment for stroke [47], and the function of mitochondrial fission on necrotic cell death has been well documented [24, 26, 48]. The uncertainty lies in the lack of genetic evidence and downstream mechanism of mitochondrial fission in necrosis [48]. Our data demonstrated that mitochondrial fragmentation occurred in necrotic neurons, and the LOF *Drp1* and *vimar* mutants both suppressed neuronal necrosis.

Much evidence suggests that the mitochondrial fusion and fission defects are directly linked to many human diseases [22], and strategies that target the Miro/vimar complex may affect a broad spectrum of diseases. For instance, mutations in the fragile X mental retardation 1 (*FMRI*) gene, which result from expansion of trinucleotide repeat in the 5' untranslated region, often cause enhanced mitochondrial fission and mental retardation syndrome [63]. Likewise, aberrant mitochondrial fusion was observed in a *Drosophila* Alzheimer's disease model induced by the ectopic expression of a human tau mutant (τ^{R406W}) [43]. In this case, the tau mutant may promote excessive actin stabilization to decrease Drp1 recruitment to the mitochondria, which results in excessive mitochondrial fusion and neurodegeneration [43, 64]. Due to the dual function of the Miro/vimar complex in high- Ca^{2+} induced necrosis and *PINK1* mutant induced PD, a drug to target this complex may benefit both disease states. As a modulator, it may be safer to target vimar/ RAP1GDS1.

Supporting Information

S1 Fig. (A) a-c, Live imaging of the mitochondrial morphology in the flight muscle of adult flies. The mitochondria are labeled with *UAS-mitoGFP* driven by *Tubulin-Gal4* (*Tubulin>mitoGFP*). The genotype is indicated on each micrograph. **d**, The averaged mitochondrial size of the control (+/+) is set as 1, and the relative ratios of the other genotypes to the control are shown. Five thoraces from each genotype were quantified. Bar graphs throughout all figures are means \pm SD. The white bar represents the control, the gray bar represents no statistical different from the control, and the black bar represents significantly different from the control. * for $p < 0.05$; ** for $p < 0.01$; *** for $p < 0.001$. (B) and (C) Vimar protein level in the adult thoraces. The Western blot shows immunoblotting with a vimar antibody, with the genotype listed on each lane. β -actin is shown as the protein loading control. The quantified data is shown as means \pm SD. Trial N = 3. (PDF)

S2 Fig. (A) Vimar distribution in other subcellular compartments. The fly homogenate was separated into cytosol, lysosome, Golgi apparatus and ER. Vimar protein level was determined by immunoblotting using a vimar antibody. Calnexin, Lamp1, GM130 and β -actin are markers for ER, lysosome, Golgi apparatus and cytoplasm, respectively. (B) Effect of *vimar* overexpression on mitochondrial transport. The mitochondria are labeled with *mitoGFP* (*CCAP>mitoGFP*), and their movements in the axons were recorded and transformed into kymographs. Overexpression of *Miro25N*, *vimar* or both of them had no effects towards mitochondria transport. Mitochondria motion in ten axons from five larvae was analyzed for each genotype. (C) Effect of *Drosophila* Miro mutants on its interaction with vimar *in vitro*. The HA-tagged Miro, Miro20V (a constitutive GTP-bound mutant) and Miro25N (a constitutive GDP-bound mutant) was individually co-transfected with Flag-tagged vimar. The co-IP experiment showed that GTP or GDP state of Miro did not affect its interaction with vimar. Trial N = 3. IgG is shown as a negative control. The total protein input is shown as the protein loading control. (PDF)

S3 Fig. (A) Effect of LOF Miro on the mitochondrial localization of vimar. In the *Mhc>mitoGFP/Miro RNAi* flies, the mitochondrial fraction of vimar was unaltered as the control *Mho>mitoGFP* flies. Anti-ATP5A is shown as the mitochondria marker and actin as cytosolic marker. Trial N = 2. (B) Live image of mitochondria in flight muscle. *Miro RNAi* and *vimar RNAi* resulted in shortened mitochondria, which could be blocked by *Drp1 RNAi*. Five thoraces from each genotype were quantified. (C) and (D) Drp1 recruitment to mitochondria in *Miro RNAi* or *vimar RNAi* background. Thoracic homogenate was separated into cytosol and mitochondria and Drp1 protein level in different fractions was immunoblotted. Anti-ATP5A is shown as the mitochondria marker and actin as cytosolic marker. Trial N = 2. (PDF)

S4 Fig. Vimar protein distribution in mitochondria fraction under high calcium stress. The AG fly heads were homogenized and separated in cytoplasmic fraction and crude mitochondria. Vimar level was labeled by a vimar antibody. Anti-ATP5A is shown as the mitochondria marker and actin as cytosolic marker. Trial N = 2. (PDF)

S5 Fig. Effect of LOF and GOF *vimar* on apoptosis. The apoptotic flies (*GMR-Gal4; GMR-Hid*) showed smaller eye size. Addition of *UAS-P35*, a known apoptosis inhibitor, is shown as a positive control, which rescued the smaller eye size defect. However, *vimar*^{k16722} or *UAS-vimar* showed no effect on the eye size defect. (PDF)

S6 Fig. Protein sequence comparison between vimar (635 a.a) and RAP1GDS1 (608 a.a). The alignment is generated from CLUSTAL alignment algorithm. (PDF)

S7 Fig. (A) Effect of the RAP1GDS1 shRNA on the level of the RAP1GDS1 protein in the stable HEK293T cells. β -actin was used as the loading control. **(B)** Effect RAP1GDS1 shRNA on necrosis in the stable SH-SY5Y cells. The cells were treated with 20 μ M A23187 for 1 hour. The bright field images of the cells showed less cell death in the RAP1GDS1 shRNA cells upon calcium ionophore treatment. Trial N = 4. **(C)** Quantification of necrosis by the ATP assay. The stable SH-SY5Y cell lines were treated with 20 μ M A23187 for 6 hours. The result showed that less cell death occurred in the RAP1GDS1 shRNA cells than the control (scrambled shRNA) cells. Trial N = 3. **(D)** The efficiency of the *Miro1* siRNA on *Miro* transcripts in 293T cells. The transcript level of *Miro1* was determined by qRT-PCR. The result showed that *Miro1* siRNA significantly knocked down *Miro1* transcripts. Trial N = 3. (PDF)

Author Contributions

Conceptualization: LD XJ LL.

Data curation: DL YH LL.

Formal analysis: LD YeL.

Investigation: LD YeL YH YuL.

Methodology: YeL YH YuL.

Project administration: LD LL.

Resources: YeL YuL.

Supervision: LL.

Writing – original draft: LD XJ LL.

Writing – review & editing: XJ.

References

1. Sheng ZH, Cai Q. Mitochondrial transport in neurons: impact on synaptic homeostasis and neurodegeneration. *Nat Rev Neurosci.* 13(2):77–93. Epub 2012/01/06. doi: nrm3156 [pii] doi: [10.1038/nrn3156](https://doi.org/10.1038/nrn3156) PMID: [22218207](https://pubmed.ncbi.nlm.nih.gov/22218207/).
2. Detmer SA, Chan DC. Functions and dysfunctions of mitochondrial dynamics. *Nat Rev Mol Cell Biol.* 2007; 8(11):870–9. doi: [10.1038/nrm2275](https://doi.org/10.1038/nrm2275) PMID: [17928812](https://pubmed.ncbi.nlm.nih.gov/17928812/).
3. Chan DC. Mitochondrial fusion and fission in mammals. *Annu Rev Cell Dev Biol.* 2006; 22:79–99. doi: [10.1146/annurev.cellbio.22.010305.104638](https://doi.org/10.1146/annurev.cellbio.22.010305.104638) PMID: [16704336](https://pubmed.ncbi.nlm.nih.gov/16704336/).
4. Westermann B. Mitochondrial fusion and fission in cell life and death. *Nat Rev Mol Cell Biol.* 2010; 11(12):872–84. doi: [10.1038/nrm3013](https://doi.org/10.1038/nrm3013) PMID: [21102612](https://pubmed.ncbi.nlm.nih.gov/21102612/).
5. Alexander C, Votruba M, Pesch UE, Thiselton DL, Mayer S, Moore A, et al. OPA1, encoding a dynamin-related GTPase, is mutated in autosomal dominant optic atrophy linked to chromosome 3q28. *Nat Genet.* 2000; 26(2):211–5. doi: [10.1038/79944](https://doi.org/10.1038/79944) PMID: [11017080](https://pubmed.ncbi.nlm.nih.gov/11017080/).
6. Chen H, Detmer SA, Ewald AJ, Griffin EE, Fraser SE, Chan DC. Mitofusins Mfn1 and Mfn2 coordinately regulate mitochondrial fusion and are essential for embryonic development. *J Cell Biol.* 2003; 160(2):189–200. doi: [10.1083/jcb.200211046](https://doi.org/10.1083/jcb.200211046) PMID: [12527753](https://pubmed.ncbi.nlm.nih.gov/12527753/); PubMed Central PMCID: [PMC2172648](https://pubmed.ncbi.nlm.nih.gov/PMC2172648/).

7. Cipolat S, Martins de Brito O, Dal Zilio B, Scorrano L. OPA1 requires mitofusin 1 to promote mitochondrial fusion. *Proc Natl Acad Sci U S A*. 2004; 101(45):15927–32. Epub 2004/10/29. doi: 10.1073/pnas.0407043101 [pii] doi: [10.1073/pnas.0407043101](https://doi.org/10.1073/pnas.0407043101) PMID: [15509649](https://pubmed.ncbi.nlm.nih.gov/15509649/); PubMed Central PMCID: PMC528769.
8. Bleazard W, McCaffery JM, King EJ, Bale S, Mozdy A, Tieu Q, et al. The dynamin-related GTPase Dnm1 regulates mitochondrial fission in yeast. *Nat Cell Biol*. 1999; 1(5):298–304. doi: [10.1038/13014](https://doi.org/10.1038/13014) PMID: [10559943](https://pubmed.ncbi.nlm.nih.gov/10559943/); PubMed Central PMCID: PMC3739991.
9. Otera H, Wang C, Cleland MM, Setoguchi K, Yokota S, Youle RJ, et al. Mff is an essential factor for mitochondrial recruitment of Drp1 during mitochondrial fission in mammalian cells. *J Cell Biol*. 2010; 191(6):1141–58. doi: [10.1083/jcb.201007152](https://doi.org/10.1083/jcb.201007152) PMID: [21149567](https://pubmed.ncbi.nlm.nih.gov/21149567/); PubMed Central PMCID: PMC3002033.
10. Guo X, Macleod GT, Wellington A, Hu F, Panchumarthi S, Schoenfield M, et al. The GTPase dMiro is required for axonal transport of mitochondria to Drosophila synapses. *Neuron*. 2005; 47(3):379–93. doi: [10.1016/j.neuron.2005.06.027](https://doi.org/10.1016/j.neuron.2005.06.027) PMID: [16055062](https://pubmed.ncbi.nlm.nih.gov/16055062/).
11. Glater EE, Megeath LJ, Stowers RS, Schwarz TL. Axonal transport of mitochondria requires miltin to recruit kinesin heavy chain and is light chain independent. *J Cell Biol*. 2006; 173(4):545–57. doi: [10.1083/jcb.200601067](https://doi.org/10.1083/jcb.200601067) PMID: [16717129](https://pubmed.ncbi.nlm.nih.gov/16717129/); PubMed Central PMCID: PMC2063864.
12. Frederick RL, McCaffery JM, Cunningham KW, Okamoto K, Shaw JM. Yeast Miro GTPase, Gem1p, regulates mitochondrial morphology via a novel pathway. *J Cell Biol*. 2004; 167(1):87–98. doi: [10.1083/jcb.200405100](https://doi.org/10.1083/jcb.200405100) PMID: [15479738](https://pubmed.ncbi.nlm.nih.gov/15479738/); PubMed Central PMCID: PMC2172521.
13. Liu S, Sawada T, Lee S, Yu W, Silverio G, Alapatt P, et al. Parkinson's disease-associated kinase PINK1 regulates Miro protein level and axonal transport of mitochondria. *PLoS Genet*. 8(3):e1002537. Epub 2012/03/08. doi: [10.1371/journal.pgen.1002537](https://doi.org/10.1371/journal.pgen.1002537) PGENETICS-D-11-02331 [pii]. PMID: [22396657](https://pubmed.ncbi.nlm.nih.gov/22396657/); PubMed Central PMCID: PMC3291531.
14. Fransson A, Ruusala A, Aspenstrom P. Atypical Rho GTPases have roles in mitochondrial homeostasis and apoptosis. *J Biol Chem*. 2003; 278(8):6495–502. doi: [10.1074/jbc.M208609200](https://doi.org/10.1074/jbc.M208609200) PMID: [12482879](https://pubmed.ncbi.nlm.nih.gov/12482879/).
15. Fransson S, Ruusala A, Aspenstrom P. The atypical Rho GTPases Miro-1 and Miro-2 have essential roles in mitochondrial trafficking. *Biochem Biophys Res Commun*. 2006; 344(2):500–10. doi: [10.1016/j.bbrc.2006.03.163](https://doi.org/10.1016/j.bbrc.2006.03.163) PMID: [16630562](https://pubmed.ncbi.nlm.nih.gov/16630562/).
16. Saotome M, Safiulina D, Szabadkai G, Das S, Fransson A, Aspenstrom P, et al. Bidirectional Ca²⁺-dependent control of mitochondrial dynamics by the Miro GTPase. *Proc Natl Acad Sci U S A*. 2008; 105(52):20728–33. doi: [10.1073/pnas.0808953105](https://doi.org/10.1073/pnas.0808953105) PMID: [19098100](https://pubmed.ncbi.nlm.nih.gov/19098100/); PubMed Central PMCID: PMC2634948.
17. Ferguson SM, De Camilli P. Dynamin, a membrane-remodelling GTPase. *Nat Rev Mol Cell Biol*. 2012; 13(2):75–88. doi: [10.1038/nrm3266](https://doi.org/10.1038/nrm3266) PMID: [22233676](https://pubmed.ncbi.nlm.nih.gov/22233676/); PubMed Central PMCID: PMC3519936.
18. Gasper R, Meyer S, Gotthardt K, Sirajuddin M, Wittinghofer A. It takes two to tango: regulation of G proteins by dimerization. *Nat Rev Mol Cell Biol*. 2009; 10(6):423–9. doi: [10.1038/nrm2689](https://doi.org/10.1038/nrm2689) PMID: [19424291](https://pubmed.ncbi.nlm.nih.gov/19424291/).
19. Cherfils J, Zeghouf M. Regulation of small GTPases by GEFs, GAPs, and GDIs. *Physiological reviews*. 2013; 93(1):269–309. doi: [10.1152/physrev.00003.2012](https://doi.org/10.1152/physrev.00003.2012) PMID: [23303910](https://pubmed.ncbi.nlm.nih.gov/23303910/).
20. Delettre C, Lenaers G, Griffoin JM, Gigarel N, Lorenzo C, Belenguer P, et al. Nuclear gene OPA1, encoding a mitochondrial dynamin-related protein, is mutated in dominant optic atrophy. *Nat Genet*. 2000; 26(2):207–10. doi: [10.1038/79936](https://doi.org/10.1038/79936) PMID: [11017079](https://pubmed.ncbi.nlm.nih.gov/11017079/).
21. Kijima K, Numakura C, Izumino H, Umetsu K, Nezu A, Shiiki T, et al. Mitochondrial GTPase mitofusin 2 mutation in Charcot-Marie-Tooth neuropathy type 2A. *Hum Genet*. 2005; 116(1–2):23–7. doi: [10.1007/s00439-004-1199-2](https://doi.org/10.1007/s00439-004-1199-2) PMID: [15549395](https://pubmed.ncbi.nlm.nih.gov/15549395/).
22. Itoh K, Nakamura K, Iijima M, Sesaki H. Mitochondrial dynamics in neurodegeneration. *Trends in cell biology*. 2013; 23(2):64–71. doi: [10.1016/j.tcb.2012.10.006](https://doi.org/10.1016/j.tcb.2012.10.006) PMID: [23159640](https://pubmed.ncbi.nlm.nih.gov/23159640/); PubMed Central PMCID: PMC3558617.
23. Knott AB, Bossy-Wetzel E. Impairing the mitochondrial fission and fusion balance: a new mechanism of neurodegeneration. *Annals of the New York Academy of Sciences*. 2008; 1147:283–92. doi: [10.1196/annals.1427.030](https://doi.org/10.1196/annals.1427.030) PMID: [19076450](https://pubmed.ncbi.nlm.nih.gov/19076450/); PubMed Central PMCID: PMC2605288.
24. Wang Z, Jiang H, Chen S, Du F, Wang X. The mitochondrial phosphatase PGAM5 functions at the convergence point of multiple necrotic death pathways. *Cell*. 2012; 148(1–2):228–43. doi: [10.1016/j.cell.2011.11.030](https://doi.org/10.1016/j.cell.2011.11.030) PMID: [22265414](https://pubmed.ncbi.nlm.nih.gov/22265414/).
25. Martorell-Riera A, Segarra-Mondejar M, Munoz JP, Ginet V, Olloquequi J, Perez-Clausell J, et al. Mfn2 downregulation in excitotoxicity causes mitochondrial dysfunction and delayed neuronal death. *EMBO J*. 2014; 33(20):2388–407. doi: [10.15252/embj.201488327](https://doi.org/10.15252/embj.201488327) PMID: [25147362](https://pubmed.ncbi.nlm.nih.gov/25147362/); PubMed Central PMCID: PMC4253527.

26. Wang W, Zhang F, Li L, Tang F, Siedlak SL, Fujioka H, et al. MFN2 couples glutamate excitotoxicity and mitochondrial dysfunction in motor neurons. *J Biol Chem.* 2015; 290(1):168–82. doi: [10.1074/jbc.M114.617167](https://doi.org/10.1074/jbc.M114.617167) PMID: [25416777](https://pubmed.ncbi.nlm.nih.gov/25416777/); PubMed Central PMCID: PMC4281719.
27. Wang X, Schwarz TL. The mechanism of Ca²⁺-dependent regulation of kinesin-mediated mitochondrial motility. *Cell.* 2009; 136(1):163–74. doi: [10.1016/j.cell.2008.11.046](https://doi.org/10.1016/j.cell.2008.11.046) PMID: [19135897](https://pubmed.ncbi.nlm.nih.gov/19135897/); PubMed Central PMCID: PMC2768392.
28. Frazier AE, Kiu C, Stojanovski D, Hoogenraad NJ, Ryan MT. Mitochondrial morphology and distribution in mammalian cells. *Biological chemistry.* 2006; 387(12):1551–8. doi: [10.1515/BC.2006.193](https://doi.org/10.1515/BC.2006.193) PMID: [17132100](https://pubmed.ncbi.nlm.nih.gov/17132100/).
29. Altmann K, Westermann B. Role of essential genes in mitochondrial morphogenesis in *Saccharomyces cerevisiae*. *Molecular biology of the cell.* 2005; 16(11):5410–7. doi: [10.1091/mbc.E05-07-0678](https://doi.org/10.1091/mbc.E05-07-0678) PMID: [16135527](https://pubmed.ncbi.nlm.nih.gov/16135527/); PubMed Central PMCID: PMC1266436.
30. Ichishita R, Tanaka K, Sugiura Y, Sayano T, Mihara K, Oka T. An RNAi screen for mitochondrial proteins required to maintain the morphology of the organelle in *Caenorhabditis elegans*. *J Biochem.* 2008; 143(4):449–54. doi: [10.1093/jb/mvm245](https://doi.org/10.1093/jb/mvm245) PMID: [18174190](https://pubmed.ncbi.nlm.nih.gov/18174190/).
31. Kikuchi A, Kaibuchi K, Hori Y, Nonaka H, Sakoda T, Kawamura M, et al. Molecular cloning of the human cDNA for a stimulatory GDP/GTP exchange protein for c-Ki-ras p21 and smg p21. *Oncogene.* 1992; 7(2):289–93. PMID: [1549351](https://pubmed.ncbi.nlm.nih.gov/1549351/).
32. Kaibuchi K, Mizuno T, Fujioka H, Yamamoto T, Kishi K, Fukumoto Y, et al. Molecular cloning of the cDNA for stimulatory GDP/GTP exchange protein for smg p21s (ras p21-like small GTP-binding proteins) and characterization of stimulatory GDP/GTP exchange protein. *Molecular and cellular biology.* 1991; 11(5):2873–80. doi: [10.1128/MCB.11.5.2873](https://doi.org/10.1128/MCB.11.5.2873) PMID: [1901951](https://pubmed.ncbi.nlm.nih.gov/1901951/); PubMed Central PMCID: PMC360075.
33. Yamamoto T, Kaibuchi K, Mizuno T, Hiroyoshi M, Shirataki H, Takai Y. Purification and characterization from bovine brain cytosol of proteins that regulate the GDP/GTP exchange reaction of smg p21s, ras p21-like GTP-binding proteins. *The Journal of biological chemistry.* 1990; 265(27):16626–34. PMID: [2118909](https://pubmed.ncbi.nlm.nih.gov/2118909/).
34. Greene JC, Whitworth AJ, Kuo I, Andrews LA, Feany MB, Pallanck LJ. Mitochondrial pathology and apoptotic muscle degeneration in *Drosophila parkin* mutants. *Proc Natl Acad Sci U S A.* 2003; 100(7):4078–83. doi: [10.1073/pnas.0737556100](https://doi.org/10.1073/pnas.0737556100) PMID: [12642658](https://pubmed.ncbi.nlm.nih.gov/12642658/); PubMed Central PMCID: PMC153051.
35. Birsa N, Norkett R, Higgs N, Lopez-Domenech G, Kittler JT. Mitochondrial trafficking in neurons and the role of the Miro family of GTPase proteins. *Biochemical Society transactions.* 2013; 41(6):1525–31. doi: [10.1042/BST20130234](https://doi.org/10.1042/BST20130234) PMID: [24256248](https://pubmed.ncbi.nlm.nih.gov/24256248/).
36. Wang X, Schwarz TL. Imaging axonal transport of mitochondria. *Methods in enzymology.* 2009; 457:319–33. doi: [10.1016/S0076-6879\(09\)05018-6](https://doi.org/10.1016/S0076-6879(09)05018-6) PMID: [19426876](https://pubmed.ncbi.nlm.nih.gov/19426876/); PubMed Central PMCID: PMC2996865.
37. Murley A, Lackner LL, Osman C, West M, Voeltz GK, Walter P, et al. ER-associated mitochondrial division links the distribution of mitochondria and mitochondrial DNA in yeast. *eLife.* 2013; 2:e00422. doi: [10.7554/eLife.00422](https://doi.org/10.7554/eLife.00422) PMID: [23682313](https://pubmed.ncbi.nlm.nih.gov/23682313/); PubMed Central PMCID: PMC3654481.
38. Kornmann B, Osman C, Walter P. The conserved GTPase Gem1 regulates endoplasmic reticulum-mitochondria connections. *Proceedings of the National Academy of Sciences of the United States of America.* 2011; 108(34):14151–6. doi: [10.1073/pnas.1111314108](https://doi.org/10.1073/pnas.1111314108) PMID: [21825164](https://pubmed.ncbi.nlm.nih.gov/21825164/); PubMed Central PMCID: PMC3161550.
39. Beall CJ, Fyrberg E. Muscle abnormalities in *Drosophila melanogaster* heldup mutants are caused by missing or aberrant troponin-I isoforms. *J Cell Biol.* 1991; 114(5):941–51. doi: [10.1083/jcb.114.5.941](https://doi.org/10.1083/jcb.114.5.941) PMID: [1908472](https://pubmed.ncbi.nlm.nih.gov/1908472/); PubMed Central PMCID: PMC2289106.
40. Babic M, Russo GJ, Wellington AJ, Sangston RM, Gonzalez M, Zinsmaier KE. Miro's N-terminal GTPase domain is required for transport of mitochondria into axons and dendrites. *J Neurosci.* 2015; 35(14):5754–71. doi: [10.1523/JNEUROSCI.1035-14.2015](https://doi.org/10.1523/JNEUROSCI.1035-14.2015) PMID: [25855186](https://pubmed.ncbi.nlm.nih.gov/25855186/); PubMed Central PMCID: PMC4388930.
41. Liu S, Sawada T, Lee S, Yu W, Silverio G, Alapatt P, et al. Parkinson's disease-associated kinase PINK1 regulates Miro protein level and axonal transport of mitochondria. *PLoS genetics.* 2012; 8(3):e1002537. doi: [10.1371/journal.pgen.1002537](https://doi.org/10.1371/journal.pgen.1002537) PMID: [22396657](https://pubmed.ncbi.nlm.nih.gov/22396657/); PubMed Central PMCID: PMC3291531.
42. Russo GJ, Louie K, Wellington A, Macleod GT, Hu F, Panchumarthi S, et al. *Drosophila* Miro is required for both anterograde and retrograde axonal mitochondrial transport. *The Journal of neuroscience: the official journal of the Society for Neuroscience.* 2009; 29(17):5443–55. doi: [10.1523/JNEUROSCI.5417-08.2009](https://doi.org/10.1523/JNEUROSCI.5417-08.2009) PMID: [19403812](https://pubmed.ncbi.nlm.nih.gov/19403812/); PubMed Central PMCID: PMC2693725.

43. DuBoff B, Gotz J, Feany MB. Tau promotes neurodegeneration via DRP1 mislocalization in vivo. *Neuron*. 2012; 75(4):618–32. doi: [10.1016/j.neuron.2012.06.026](https://doi.org/10.1016/j.neuron.2012.06.026) PMID: [22920254](https://pubmed.ncbi.nlm.nih.gov/22920254/); PubMed Central PMCID: [PMC3428596](https://pubmed.ncbi.nlm.nih.gov/PMC3428596/).
44. Verstreken P, Ly CV, Venken KJ, Koh TW, Zhou Y, Bellen HJ. Synaptic mitochondria are critical for mobilization of reserve pool vesicles at *Drosophila* neuromuscular junctions. *Neuron*. 2005; 47(3):365–78. doi: [10.1016/j.neuron.2005.06.018](https://doi.org/10.1016/j.neuron.2005.06.018) PMID: [16055061](https://pubmed.ncbi.nlm.nih.gov/16055061/).
45. Liu K, Ding L, Li Y, Yang H, Zhao C, Lei Y, et al. Neuronal necrosis is regulated by a conserved chromatin-modifying cascade. *Proc Natl Acad Sci U S A*. 2014; 111(38):13960–5. doi: [10.1073/pnas.1413644111](https://doi.org/10.1073/pnas.1413644111) PMID: [25201987](https://pubmed.ncbi.nlm.nih.gov/25201987/).
46. Kohda K, Wang Y, Yuzaki M. Mutation of a glutamate receptor motif reveals its role in gating and delta2 receptor channel properties. *Nat Neurosci*. 2000; 3(4):315–22. doi: [10.1038/73877](https://doi.org/10.1038/73877) PMID: [10725919](https://pubmed.ncbi.nlm.nih.gov/10725919/).
47. Grohm J, Kim SW, Mamrak U, Tobaben S, Cassidy-Stone A, Nunnari J, et al. Inhibition of Drp1 provides neuroprotection in vitro and in vivo. *Cell Death Differ*. 2012; 19(9):1446–58. doi: [10.1038/cdd.2012.18](https://doi.org/10.1038/cdd.2012.18) PMID: [22388349](https://pubmed.ncbi.nlm.nih.gov/22388349/); PubMed Central PMCID: [PMC3422469](https://pubmed.ncbi.nlm.nih.gov/PMC3422469/).
48. Jahani-Asl A, Germain M, Slack RS. Mitochondria: joining forces to thwart cell death. *Biochimica et biophysica acta*. 2010; 1802(1):162–6. doi: [10.1016/j.bbdis.2009.09.006](https://doi.org/10.1016/j.bbdis.2009.09.006) PMID: [19747972](https://pubmed.ncbi.nlm.nih.gov/19747972/).
49. Clark IE, Dodson MW, Jiang C, Cao JH, Huh JR, Seol JH, et al. *Drosophila* pink1 is required for mitochondrial function and interacts genetically with parkin. *Nature*. 2006; 441(7097):1162–6. doi: [10.1038/nature04779](https://doi.org/10.1038/nature04779) PMID: [16672981](https://pubmed.ncbi.nlm.nih.gov/16672981/).
50. Bergmann A, Agapite J, McCall K, Steller H. The *Drosophila* gene hid is a direct molecular target of Ras-dependent survival signaling. *Cell*. 1998; 95(3):331–41. doi: [10.1016/S0092-8674\(00\)81765-1](https://doi.org/10.1016/S0092-8674(00)81765-1) PMID: [9814704](https://pubmed.ncbi.nlm.nih.gov/9814704/).
51. Lo PC, Frasch M. bagpipe-Dependent expression of vimar, a novel Armadillo-repeats gene, in *Drosophila* visceral mesoderm. *Mech Dev*. 1998; 72(1–2):65–75. doi: [10.1016/S0925-4773\(98\)00016-1](https://doi.org/10.1016/S0925-4773(98)00016-1) PMID: [9533953](https://pubmed.ncbi.nlm.nih.gov/9533953/).
52. Karch J, Kwong JQ, Burr AR, Sargent MA, Elrod JW, Peixoto PM, et al. Bax and Bak function as the outer membrane component of the mitochondrial permeability pore in regulating necrotic cell death in mice. *eLife*. 2:e00772. Epub 2013/08/31. doi: [10.7554/eLife.00772](https://doi.org/10.7554/eLife.00772) 00772 [pii]. PMID: [23991283](https://pubmed.ncbi.nlm.nih.gov/23991283/); PubMed Central PMCID: [PMC3755340](https://pubmed.ncbi.nlm.nih.gov/PMC3755340/).
53. Degterev A, Huang Z, Boyce M, Li Y, Jagtap P, Mizushima N, et al. Chemical inhibitor of nonapoptotic cell death with therapeutic potential for ischemic brain injury. *Nature chemical biology*. 2005; 1(2):112–9. doi: [10.1038/nchembio711](https://doi.org/10.1038/nchembio711) PMID: [16408008](https://pubmed.ncbi.nlm.nih.gov/16408008/).
54. Chen J, Shi X, Padmanabhan R, Wang Q, Wu Z, Stevenson SC, et al. Identification of novel modulators of mitochondrial function by a genome-wide RNAi screen in *Drosophila melanogaster*. *Genome Res*. 2008; 18(1):123–36. Epub 2007/11/29. doi: [gr.6940108](https://doi.org/gr.6940108) [pii] doi: [10.1101/gr.6940108](https://doi.org/10.1101/gr.6940108) PMID: [18042644](https://pubmed.ncbi.nlm.nih.gov/18042644/); PubMed Central PMCID: [PMC2134776](https://pubmed.ncbi.nlm.nih.gov/PMC2134776/).
55. Westermann B. Bioenergetic role of mitochondrial fusion and fission. *Biochimica et biophysica acta*. 2012; 1817(10):1833–8. doi: [10.1016/j.bbabi.2012.02.033](https://doi.org/10.1016/j.bbabi.2012.02.033) PMID: [22409868](https://pubmed.ncbi.nlm.nih.gov/22409868/).
56. Narendra DP, Jin SM, Tanaka A, Suen DF, Gautier CA, Shen J, et al. PINK1 is selectively stabilized on impaired mitochondria to activate Parkin. *PLoS biology*. 2010; 8(1):e1000298. doi: [10.1371/journal.pbio.1000298](https://doi.org/10.1371/journal.pbio.1000298) PMID: [20126261](https://pubmed.ncbi.nlm.nih.gov/20126261/); PubMed Central PMCID: [PMC2811155](https://pubmed.ncbi.nlm.nih.gov/PMC2811155/).
57. Matsuda N, Sato S, Shiba K, Okatsu K, Saisho K, Gautier CA, et al. PINK1 stabilized by mitochondrial depolarization recruits Parkin to damaged mitochondria and activates latent Parkin for mitophagy. *The Journal of cell biology*. 2010; 189(2):211–21. doi: [10.1083/jcb.200910140](https://doi.org/10.1083/jcb.200910140) PMID: [20404107](https://pubmed.ncbi.nlm.nih.gov/20404107/); PubMed Central PMCID: [PMC2856912](https://pubmed.ncbi.nlm.nih.gov/PMC2856912/).
58. Ziviani E, Tao RN, Whitworth AJ. *Drosophila* parkin requires PINK1 for mitochondrial translocation and ubiquitinates mitofusin. *Proc Natl Acad Sci U S A*. 2010; 107(11):5018–23. doi: [10.1073/pnas.0913485107](https://doi.org/10.1073/pnas.0913485107) PMID: [20194754](https://pubmed.ncbi.nlm.nih.gov/20194754/); PubMed Central PMCID: [PMC2841909](https://pubmed.ncbi.nlm.nih.gov/PMC2841909/).
59. Park J, Lee SB, Lee S, Kim Y, Song S, Kim S, et al. Mitochondrial dysfunction in *Drosophila* PINK1 mutants is complemented by parkin. *Nature*. 2006; 441(7097):1157–61. doi: [10.1038/nature04788](https://doi.org/10.1038/nature04788) PMID: [16672980](https://pubmed.ncbi.nlm.nih.gov/16672980/).
60. Macaskill AF, Rinholm JE, Twelvetrees AE, Arancibia-Carcamo IL, Muir J, Fransson A, et al. Miro1 is a calcium sensor for glutamate receptor-dependent localization of mitochondria at synapses. *Neuron*. 2009; 61(4):541–55. doi: [10.1016/j.neuron.2009.01.030](https://doi.org/10.1016/j.neuron.2009.01.030) PMID: [19249275](https://pubmed.ncbi.nlm.nih.gov/19249275/); PubMed Central PMCID: [PMC2670979](https://pubmed.ncbi.nlm.nih.gov/PMC2670979/).
61. Chen Y, Sheng ZH. Kinesin-1-syntrophin coupling mediates activity-dependent regulation of axonal mitochondrial transport. *The Journal of cell biology*. 2013; 202(2):351–64. doi: [10.1083/jcb.201302040](https://doi.org/10.1083/jcb.201302040) PMID: [23857772](https://pubmed.ncbi.nlm.nih.gov/23857772/); PubMed Central PMCID: [PMC3718985](https://pubmed.ncbi.nlm.nih.gov/PMC3718985/).

62. Cassidy-Stone A, Chipuk JE, Ingeman E, Song C, Yoo C, Kuwana T, et al. Chemical inhibition of the mitochondrial division dynamin reveals its role in Bax/Bak-dependent mitochondrial outer membrane permeabilization. *Dev Cell*. 2008; 14(2):193–204. doi: [10.1016/j.devcel.2007.11.019](https://doi.org/10.1016/j.devcel.2007.11.019) PMID: [18267088](https://pubmed.ncbi.nlm.nih.gov/18267088/); PubMed Central PMCID: [PMC2267902](https://pubmed.ncbi.nlm.nih.gov/PMC2267902/).
63. Ross-Inta C, Omanska-Klusek A, Wong S, Barrow C, Garcia-Arocena D, Iwahashi C, et al. Evidence of mitochondrial dysfunction in fragile X-associated tremor/ataxia syndrome. *The Biochemical journal*. 2010; 429(3):545–52. doi: [10.1042/BJ20091960](https://doi.org/10.1042/BJ20091960) PMID: [20513237](https://pubmed.ncbi.nlm.nih.gov/20513237/); PubMed Central PMCID: [PMC4011071](https://pubmed.ncbi.nlm.nih.gov/PMC4011071/).
64. Fulga TA, Elson-Schwab I, Khurana V, Steinhilb ML, Spires TL, Hyman BT, et al. Abnormal bundling and accumulation of F-actin mediates tau-induced neuronal degeneration in vivo. *Nat Cell Biol*. 2007; 9(2):139–48. doi: [10.1038/ncb1528](https://doi.org/10.1038/ncb1528) PMID: [17187063](https://pubmed.ncbi.nlm.nih.gov/17187063/).